

Globular Cluster Systems in Four BCGs: A262, A3560, A3565 and A3742 ¹

Waldemar M. Okoń and William E. Harris

*Department of Physics and Astronomy, McMaster University, Hamilton, ON L8S 4M1,
Canada; okon@physics.mcmaster.ca, harris@physics.mcmaster.ca*

ABSTRACT

We have used deep *I*-band (F814W) images from the HST archive to study the globular cluster systems around the brightest cluster galaxies (BCGs) in Abell 262, 3560, 3565 and 3742. Three of these BCGs have inner dust lanes and peculiar structural features which indicate past histories of low-level interaction and accretion. The deep *I*-band WFPC2 images have photometric limits which, for all four galaxies, reach near or just beyond the GCLF turnover point. Their specific frequencies are 8.24 ± 1.65 , 4.66 ± 0.93 , 2.58 ± 0.52 and 2.62 ± 0.52 respectively, all within a factor of two of the normal range for giant ellipticals. We obtain new estimates of the GCLF turnover magnitudes, which are shown to be consistent with an adopted Hubble constant of $H_0 \simeq 70 \text{ km s}^{-1} \text{ Mpc}^{-1}$ on the “Hubble diagram” of GCLF turnover apparent magnitude versus redshift, on a distance scale where the fundamental GCLF calibrator E galaxies (M87 and others) in Virgo are at $d = 16 \text{ Mpc}$.

Subject headings: galaxies: elliptical and cD — galaxies: evolution — galaxies: individual (A262, A3560, A3565, A3742) — galaxies: star clusters — galaxies: structure

1. Introduction

Globular clusters are found in their largest numbers within giant elliptical and cD galaxies. While the clusters constitute only a small fraction of a galaxy halo’s mass, they are the

¹Based on observations with the NASA/ESA Hubble Space Telescope, obtained at the Space Telescope Science Institute, which is operated by the Association of Universities for Research in Astronomy, Inc., under NASA contract NAS 5-26555. These observations are associated with proposal ID 5910.

most easily identified surviving structures of the initial stages of galaxy formation. This makes them important tracers of galaxy formation models. From deep wide-field imaging, several features of the globular cluster system can readily be derived, including the radial distribution, luminosity distribution, and the total population (specific frequency S_N).

In this paper we obtain measurements of the globular cluster systems (GCSs) in the central giant E galaxies within four Abell galaxy clusters in the redshift range $cz \sim 4000 - 4700 \text{ km s}^{-1}$. These are NGC 708 in A262, NGC 5193 in A3560, IC 4296 in A3565 and NGC 7014 in A3742. The raw data are WFPC2 I -band exposures drawn from the HST archive. Preliminary studies of these systems were made by Lauer et al. (1998), but using only the PC1 chip data; we make use of all the WFPC2 data available, more than doubling the amount of information on the globular cluster luminosity function (GCLF) in each galaxy, and also enabling us to study the GCS radial distributions and specific frequencies with much higher confidence. Finally, using the GCLF turnover magnitude and redshift of these galaxies and others in the literature, we construct a purely GCLF-based Hubble diagram and show that it is consistent with $H_0 = 70$.

2. Data Reduction

The original images were taken in the F814W filter by Lauer et al. (1998) with the WFPC2 camera, between January and April 1996 (Program ID 5910). The target galaxies were centered in the high resolution PC1 chip, hence maximizing the total globular cluster population falling within the field of view of the entire camera. The exposures (totaling between 9200 and 16500 s) were sub-pixel-shifted. With standard IRAF and STSDAS routines, we co-added each group to reconstruct clean composite images free of bad pixel artifacts and cosmic ray contamination.

Various small areas on each image were masked out in subsequent analysis to eliminate contamination from diffraction spikes of bright stars, or neighboring galaxies in the field. Also, the innermost parts of the target galaxies themselves were masked out, within radii of $3.''7$, $3.''8$, $5.''8$ and $2.''8$ from the centers of the galaxies respectively.

We next subtracted background light from the combined images. For this purpose we used a simple median filter on the WF2,3,4 fields, where the background light gradient is low. However, for the PC1 chip, we fitted elliptical isophotes (using STSDAS and ELLIPSE) to the galaxy, generating synthetic isophotal contours which were then subtracted from the original.

With the galaxy light subtracted, we found that some of the galaxies exhibited various

types of interesting substructure. The most prominent of these is the inner region of NGC 708, which exhibits an easily seen dust lane (see the illustrations of each one shown in Lauer et al.). Smaller dust lanes were also detected within NGC 5193 and IC 4296, indicating likely accretion events in the recent past. Giovanelli et al. (1982) found that A262, the host cluster for NGC 708, contains galaxies deficient of HI gas, suggested as due to ram-pressure stripping. This gas could be accreted by the central cD galaxy, with its large dark halo. A262 is a spiral-rich cluster, characterized by a X-ray source, 3U 015+36, which appears concentric with the central galaxy. The gas and galaxy virial temperatures for the cluster have recently been shown to be comparable by Neill et al. (2001). There seems to be a general pattern for HI deficiency to be associated with X-ray emission, some other examples being A2147 in Hercules, or Coma.

Our procedures for photometry of the four combined images follow the basic sequence outlined in more detail elsewhere (e.g., Woodworth & Harris (2000), Kavelaars et al. (2000)). Of the many detected faint starlike objects on the frames, the vast majority are globular clusters within the BCGs. At these distances (~ 55 Mpc) they appear as unresolved point sources, even in the PC1 frames. Hence, it is easy to perform conventional point-spread function (PSF) photometry on the frames. Independent empirical PSFs were constructed from several moderately bright, uncrowded stars in each of the four WFPC2 frames with DAOPHOT. Then ALLSTAR (Stetson 1994) was used to generate the final photometry. A standard detection threshold of 3.5 times the rms scatter of the sky background was adopted for the image detection. Crowding at all magnitudes was completely negligible in these high-latitude fields.

An image classification algorithm (CLASSIFY; defined by Kron (1980) and Harris et al. (1991)) was then used to calculate radial image moments of the candidate objects and thus to separate stellar from nonstellar objects in an objective way. By using artificial-star data passed through exactly the same measurement process, we established boundaries for the CLASSIFY parameters such that at least 95% of the true stars were retrieved at all magnitudes (for very similar examples with illustrative graphs, see Woodworth & Harris (2000) and Kavelaars et al. (2000)). As usual, for the faintest objects the image moments become very uncertain, and it becomes difficult to distinguish between stellar and nonstellar objects. Also, some nonstellar objects will be accidentally classified as stellar. These are statistically removed from the final GCLF by subtracting a background luminosity function (see below).

Finally, to define the photometric completeness function we constructed annular rings around the BCGs, and employed extensive artificial-star tests to measure the detection completeness $f(m, r)$, as a function of magnitude and radial distance. In practice we found

that the PC1 chip with its strong background light gradient was the only area where f was a significant function of radius; on the WF chips a single function $f(m)$ could be used.

The instrumental magnitudes were converted to the Johnson-Cousins I system with the standard transformations for $F814W$ found in Holtzman et al. (1995). For the four individual BCGs, Galactic extinction corrections of $A_I = 0.16, 0.10, 0.11$ and 0.06 respectively have been adopted (A_I is given by $A_I = 1.82 E_{B-V}$, where the E_{B-V} values are obtained for each galaxy from NASA/IPAC Extragalactic Database (NED)). To employ the transformation equations and also to step back and forth between I and the (more normally used) V magnitude scale for globular clusters, we have simply assumed a color index of $(V - I)_0 = 1.1 \pm 0.1$, typical of moderately metal-rich globular clusters in giant E galaxies (e.g. Kundu et al. (1999)). The intrinsic range in $(V - I)_0$, folded through the transformation equations, will not introduce uncertainties larger than ± 0.03 in the calibration of I . The assumed $(V - I)_0$ value is the mean value representative of most other gE galaxies, and if the GCSs were entirely metal-rich or metal-poor, the error introduced by the assumption would be at most 0.1 mag.

3. Analysis and Discussion

3.1. Radial Profiles

The projected number density σ of detected objects around each galaxy plainly reveals an extensive GCS concentrated around the galaxy center in each case. The profile is reasonably well represented by a simple power-law form $\sigma(r) = \sigma_{cl}(r) + \sigma_{bg} = a r^b + \sigma_{bg}$, where σ_{bg} is the background number density of starlike objects (mostly faint, small galaxies which passed through the image classification routines, plus a few foreground Galactic stars). To obtain the profile parameters of the GCS for each galaxy, we subdivided the WFPC2 fields into annuli 50 pixels wide, centered on the BCGs. The number density of objects was then calculated down to a cutoff magnitude at which incompleteness corrections were still small. The projected number density is then just $\sigma = N/A$, where N is the number of detected objects within each annulus and A is the area of that annulus which falls within the WFPC2 boundaries (minus the small masked-out areas). Completeness corrections, though small, were explicitly accounted for. Finally, the background density σ_{bg} on each of the four fields was defined as the mean of the outermost eight annuli, which fall on the outskirts of the WF chips. This corresponds to a radial distance greater than $105''$ (or about 30 kpc) from the centers of the BCGs. Although the GCSs probably extend at trace amounts farther out than this boundary, the directly observed $\sigma(r)$ curves (Figure 1) have plainly almost leveled off there, indicating that we are already including the main portion of the GCS.

Figure 2 shows log-log plots of the background-subtracted density profiles for the four BCGs, and Table 1 lists our deduced values for the power-law index b , as well as the adopted σ_{bg} . We note the bumpiness of the $\sigma_{cl}(r)$ curve for NGC 708 in Abell 262. It exhibits a clear peak around 1.25, and a less clear peak around 0.6. If not simply statistical fluctuations, these could be the result of uncompensated background contamination (clumpiness in the distribution of faint, ultra-distant galaxy clusters, or even some residual globular cluster populations which belong to neighboring galaxies in A262; there are several smaller elliptical galaxies as well as a companion spiral in the WFPC2 field).

Also, the slope of the $\sigma_{cl}(r)$ curve for IC 4296 in A3565 declines smoothly out to about 1.5, and then exhibits a relatively sharp drop-off. This effect is not apparent in the other three systems. It is possible that this feature, if real (and not just a prosaic result of overestimating the background count), is due to tidal truncation. There are no large nearby galaxies in the immediate vicinity of IC 4296. However, Mulchaey et al. (1996) in a *ROSAT* study of groups and poor clusters find that the X-ray contours in A3565 are not centered on the BCG, but rather at a point roughly halfway between IC 4296 and the neighboring spiral IC 4299. The mass that Mulchaey et al. (1996) have derived for the X-ray gas is about one-third of the mass of the entire cluster derived from the galaxy velocity distribution (Willmer et al. 1999). It might therefore be possible that the BCG oscillates about the center of the potential well of the cluster, which could be responsible for the truncation of its halo.

For luminous giant E galaxies like these, the GCS profile shape is expected to be rather flat, becoming more shallow as galaxy luminosity increases. A general relation for the power-law slope is (Kaisler et al. 1996).

$$b = -0.29 M_V^T - 8.00$$

The only one of our four target BCGs which deviates fairly strongly from this empirical relation is NGC 708 (an observed slope $b = -1.0$ versus an expected one of -1.7). It is, however, the only one in our sample with a cD envelope, which has clearly made it more radially extended than normal.

3.2. Globular Cluster Luminosity Function

The globular cluster luminosity function (GCLF) is conventionally defined as the number of globular clusters per unit magnitude. In this form it has a unimodal and nearly symmetric shape, and for analytical purposes can be reasonably approximated by a Gaussian function (cf. Harris (2001) for extensive discussion and background). For giant elliptical galaxies the

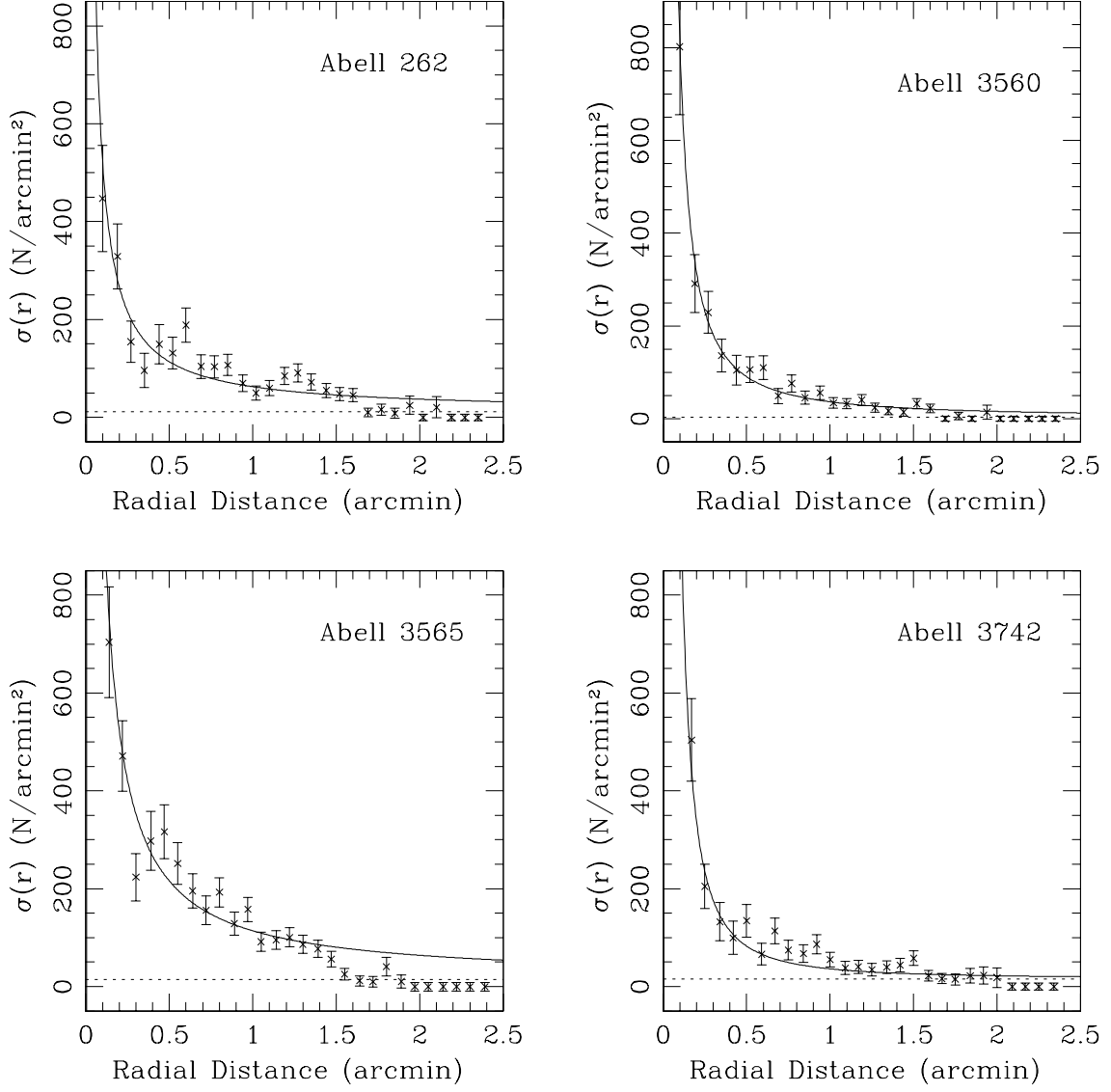


Fig. 1.— Radial profiles of the detected starlike objects around the four target BCGs. The dotted lines indicate the adopted background density levels, defined as the mean of the outermost annuli.

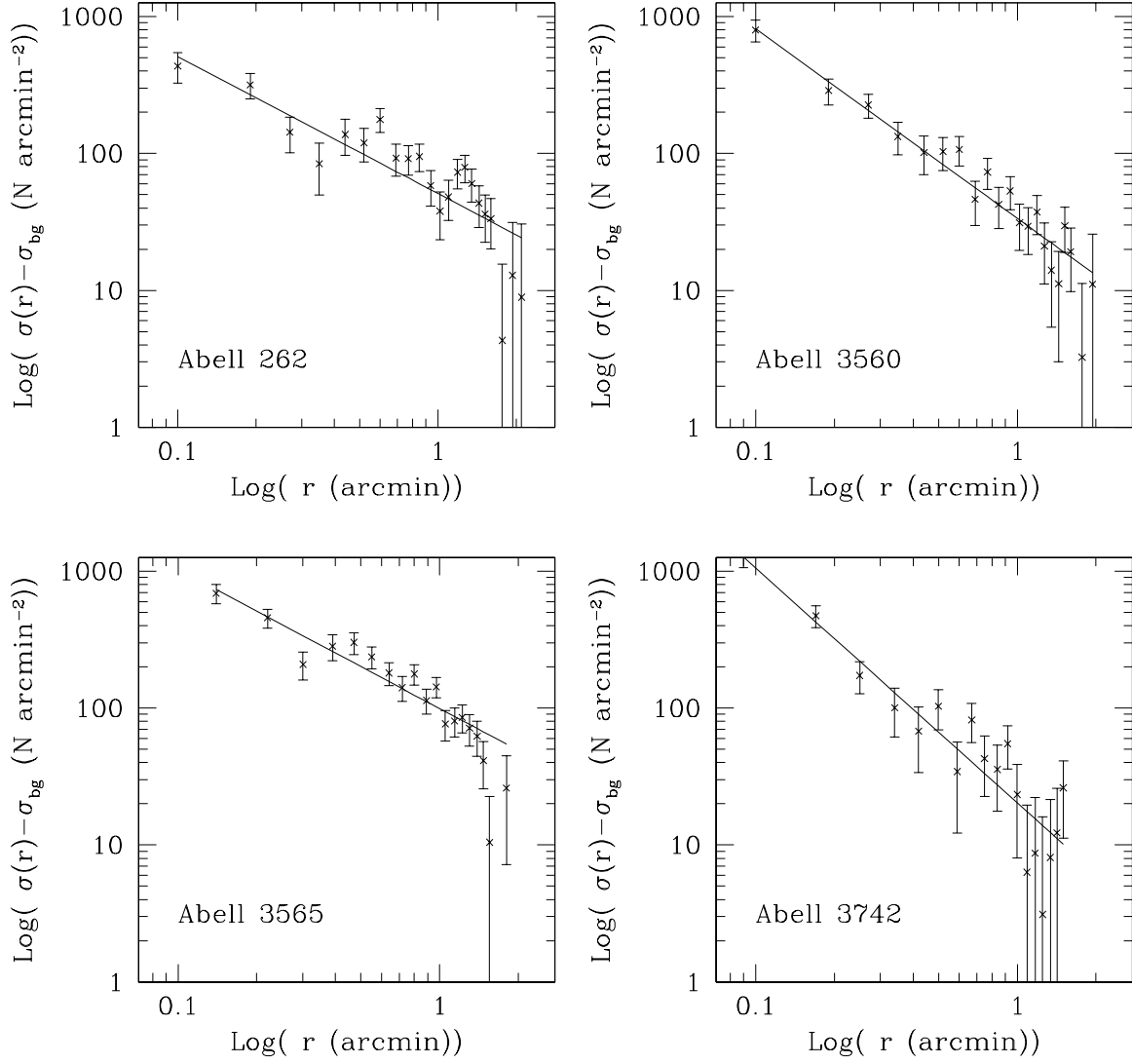


Fig. 2.— Log-log plot of radial profiles of the detected starlike objects around the four target BCGs. The background density, σ_{bg} , has been subtracted.

Table 1: Radial Density Profile Data

Galaxy	b	σ_{bg}
N708 (A262)	-1.00 ± 0.11	11.6 ± 3.1
N5193 (A3560)	-1.38 ± 0.07	2.8 ± 1.9
I4296 (A3565)	-1.02 ± 0.08	15.0 ± 3.9
N7014 (A3742)	-1.71 ± 0.11	16.0 ± 3.6

Gaussian dispersion σ_V of the distribution is found to be 1.36 ± 0.03 (see below) while the peak frequency, also known as the GCLF turnover point, is equal to $M_V^0 = -7.33 \pm 0.04$ on a distance scale where the calibrating ellipticals (M87 and others in the Virgo cluster) are at $d = 16$ Mpc (see Harris (2001); Kavelaars et al. (2000)). The demonstrated small galaxy-to-galaxy spread in M_V^0 makes it an interesting standard candle for distance measurements, because it is detectable to distances beyond which peculiar motions of galaxies bias the Hubble flow (see §3.5).

To plot the GCLFs for our four GCSs, we have used completeness-corrected totals in 0.25 mag bins above the 50% completeness level magnitudes. A background GCLF was statistically subtracted, defined from the objects (mostly background galaxies) in the outskirts of the fields (same region as the one used to define σ_{bg} above). The best-fit Gaussian function was obtained with a constrained χ^2 minimization method.

When solving for the two important GCLF parameters (the apparent magnitude of the turnover, in this case I^0 , and the dispersion σ_I), it is important to note that their solutions are correlated (see Secker & Harris (1993); Hanes & Whittaker (1987); Kavelaars et al. (2000)). If, as is true in our case, the photometric limit $I(lim)$ is close to or just past the true turnover magnitude, the fitted values for the turnover and dispersion are constrained from only one side (the bright end). In this situation, attempts to solve simultaneously for the turnover and the dispersion tend to produce overestimates of both quantities. One can obtain a *systematically* more accurate fit by adopting a fiducial value for the dispersion, and solving only for the turnover magnitude. Fortunately, it has been shown (see Whitmore (1996) and Harris (2001)) for more than a dozen gE galaxies with well measured GCLFs, that the dispersion is very consistent from one galaxy to another, with $\langle \sigma_V \rangle = 1.36 \pm 0.10$ rms scatter. We adopt that dispersion value here and solve only for the turnover magnitudes I^0 .

Our full completeness-corrected and background-subtracted luminosity functions, along

with the fitted Gaussian functions (assuming $\sigma_I = 1.36$) are shown in Figure 3. The individual points were weighted as $(n/e(n))^2$ where n and $e(n)$ denote the number of objects in the bin and the internal uncertainty. Table 2 lists the resulting turnover I -magnitudes obtained for the GCLFs, with successive columns giving the result from (a) only the PC1 data, (b) only the WF data, (c) all data combined, and finally (d) the values determined previously by Lauer et al. The V^0 values result from the fitted I^0 once we add our adopted mean color index $(V - I)_0 = 1.1 \pm 0.1$. In the Table, the quoted I^0 values have had Galactic extinction subtracted. The quoted uncertainties in the Table represent only the *internal* uncertainty of the fitting procedure.

Our results for the four BCGs yield turnover magnitudes quite similar to those obtained by Lauer et al. (1998) for A262, A3742, but fainter than their values for A3560 and A3565. Lauer et al. employed the same basic fitting curve (a Gaussian with dispersion 1.4 magnitudes), but there are two notable differences between their analysis and ours. First, we have used all the available WFPC2 data (not just the PC1 data), more than doubling the total cluster populations used in the fit. Second, there are important differences of detail in the fitting procedure. We define an *empirical* background LF from the outer parts of the images; then subtract this background from the total number counts; and then fit the (residual) LF with the model Gaussian function. By contrast, Lauer et al. fit a model to the raw data which includes both the assumed Gaussian GCLF shape and a model background LF which rises smoothly and exponentially with magnitude. Either procedure depends for its accuracy on the correctness of the assumed background LF particularly at faint levels. Thus, for example, if their background model overestimated the true background at or beyond the true GCLF turnover, it would yield an I^0 which was artificially too bright. In cases such as these where the photometric limit is very close to the actual turnover, the true (external) uncertainty in I^0 is likely to be closer to ± 0.3 magnitude (cf. the references cited above). However, primarily because of the much larger GCLF sample size in our data and our locally determined backgrounds, we believe our turnover determinations to be improvements over the previous work.²

In Figure 4 we show the GCLF from our data broken separately into the WF and PC1 data (and with separate fitted Gaussians for both subsets). Notably, the fits from the PC1 data alone yield consistently brighter turnovers than do the deeper WF data, indicating the importance of obtaining photometric limits at or beyond the actual turnover to avoid

²We have compared the GCLFs from only our PC1 data directly with those of Lauer et al. (see their Figure 8). After correction for the different bin sizes, we find that their actual GCLF datapoints and ours agree quite closely, to well within the internal errors of either set. Our PC1 data do not reach as faint as theirs, however, indicating that our detection threshold was more conservative.

systematic errors. The WF data have limiting magnitudes similar to those of Lauer et al., and the turnover magnitudes we deduced from the WF data alone are generally closer to those deduced by Lauer et al., as are those from the total (PC+WF) dataset. These latter fits are certainly to be preferred over the PC1 data alone.

We note that the datapoints in the faintest bin for A262, A3560 and A3742 in Figure 3 and in the WF Figure 4 fall clearly below the fitted GCLF curve. This does not appear to be due to an incorrect completeness correction at that level. The only other obvious possibility is that our empirical background has been overestimated in the last bin, but it is unclear whether that is the case without deeper data to draw on.

Table 2: GCLF Turnover Magnitudes

Galaxy	$I^0(\text{PC1})$	$I^0(\text{WF})$	$I^0(\text{total})$	$I^0(\text{Lauer et al.})$
N708 (A262)	24.66	25.90	25.74 ± 0.17	25.85 ± 0.25
N5193 (A3560)	24.62	25.81	25.81 ± 0.18	25.12 ± 0.25
I4296 (A3565)	24.66	25.72	25.54 ± 0.16	24.72 ± 0.25^1
N7014 (A3742)	25.58	25.71	25.66 ± 0.19	25.77 ± 0.25

¹ The turnover magnitude for IC 4296 listed by Lauer et al. (1998) in their Table 2 ($I_0 = 25.72$) is a typographical error. It should read $I^0 = 24.72$, which is the value from their graph (Figure 8) (Lauer 2001).

3.3. Luminosity and Mass Distribution Functions

The luminosity distribution function (LDF), or number of clusters per unit *luminosity* (dN/dL), is the visible signature of the cluster mass distribution and is a more physically oriented representation of the GCLF. In this plane it usually appears as a rough power law, $dN/dL \sim L^{-\alpha_L}$. By adopting a mass-to-light ratio one can also immediately obtain the mass distribution function $dN/dM \sim M^{-\alpha_M}$, where $\alpha_L \simeq \alpha_M$ as long as the M/L ratio is roughly independent of cluster mass (see Mandushev et al. (1991) and McLaughlin (2000)).

It has been noted many times that within observational uncertainty, the globular cluster mass distribution follows a simple power law relation which has the same shape as the mass distribution of giant molecular clouds (GMCs) in large spirals, cloud cores embedded in GMCs, and giant HII regions in large spirals (e.g. Harris & Pudritz (1994) and subsequent papers). The power-law slope α_M falls consistently in the range 1.8 ± 0.2 for $L > 10^5 L_\odot$, a

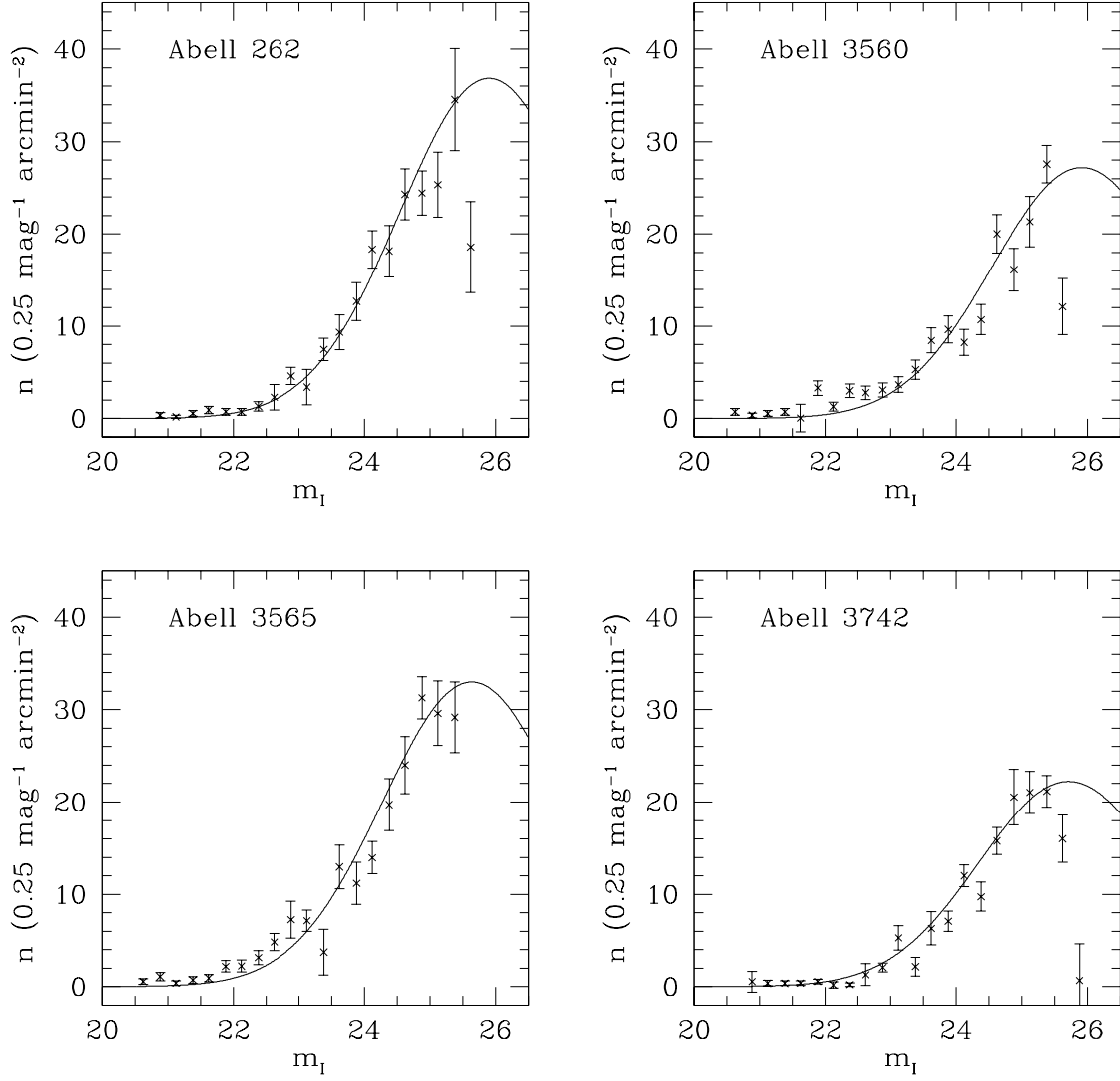


Fig. 3.— The data defining the globular cluster luminosity function (GCLF) for bins brighter than the 50% completeness level. The solid lines are Gaussians of width $\sigma_V = 1.36$.

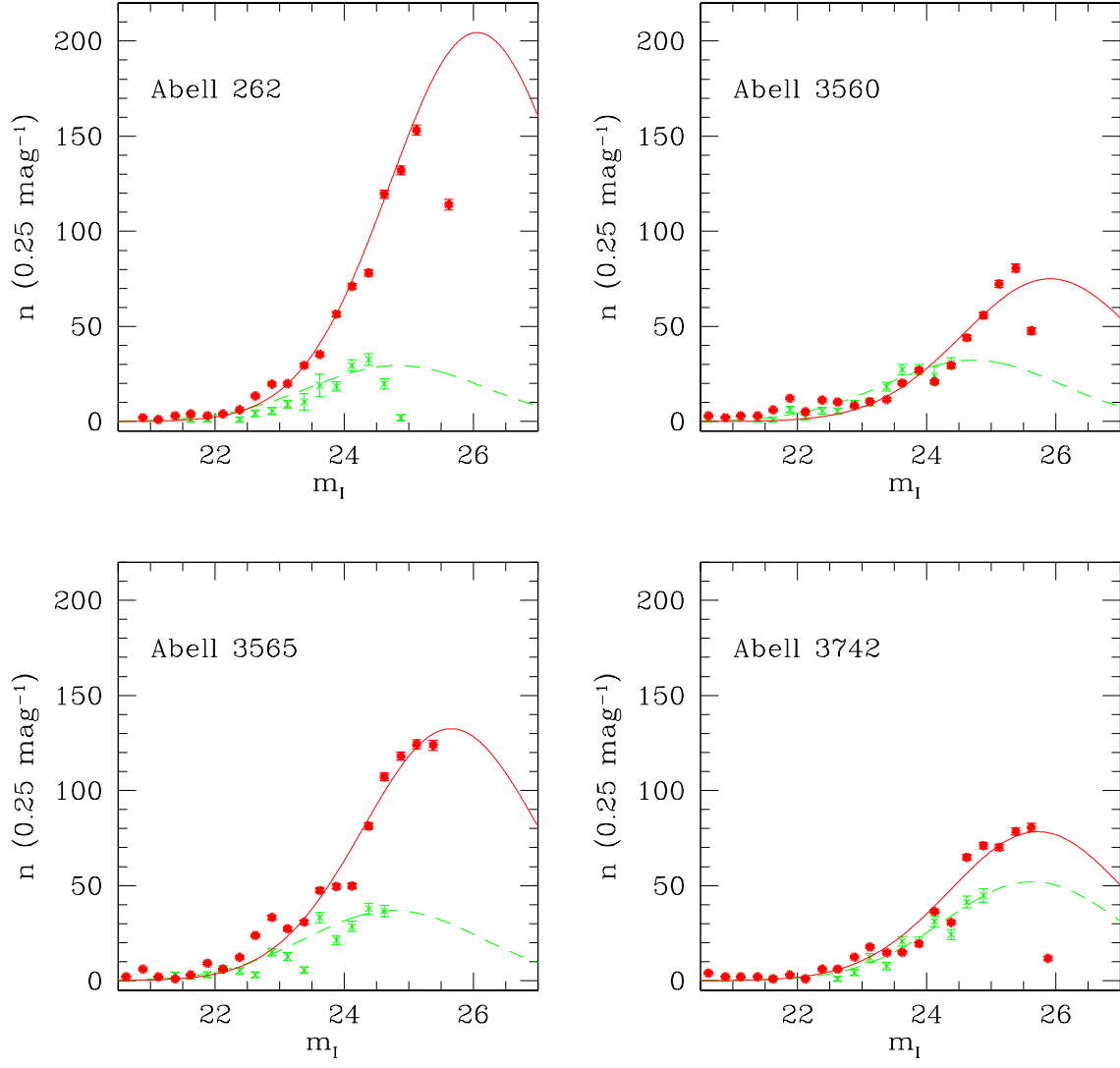


Fig. 4.— The data defining the globular cluster luminosity functions (GCLFs) for bins above the 50% completeness level on the PC1 (dashed) and WF (solid) chips. The fitted lines are Gaussians of width $\sigma_V = 1.36$.

value which can be at least approximately explained by cluster formation pictures ranging from collisional growth of protocluster gas clouds (McLaughlin & Pudritz 1996) to turbulence spectra (Elmegreen & Efremov 1997).

Here we define the LDFs observationally in a separate procedure from the GCLF: we convert the apparent magnitudes of the detected objects to absolute magnitudes M_V using the galaxy distance moduli and adopted cluster color, and then to luminosities L_V . The background LDF is subtracted and the data binned in steps of $10^5 L_\odot$. For the mass distribution function we have multiplied the luminosity values by a mass-to-light ratio $M/L_V = 1.45$ (McLaughlin 2000) and binned the data in steps of $10^5 M_\odot$.

We note that the lowest luminosity (and hence mass) point for each of the functions has been excluded from the fits. This corresponds to a point $L < 10^5 L_\odot$, since at this luminosity, the slope of the power law relation changes for the distribution function (see McLaughlin (1994)).

Figure 5 shows the LDFs which we have obtained for the four galaxies. Table 3 lists the values obtained for the slopes of the power law relations of the luminosity and mass distribution functions, α_L and α_M . (These are slightly but not significantly different in each pair because of the different bin boundary locations in L and M .) With the exception of NGC 5193 in A3560 which has a value of α_M notably lower than the expected 1.8 ± 0.2 , the other three galaxies are entirely consistent with the other giant ellipticals in Virgo, Fornax and elsewhere.

Table 3: Luminosity and Mass Distribution Function Data

Galaxy	α_L	α_M
N708 (A262)	-1.97 ± 0.11	-1.86 ± 0.08
N5193 (A3560)	-1.57 ± 0.07	-1.48 ± 0.05
I4296 (A3565)	-1.85 ± 0.07	-1.74 ± 0.07
N7014 (A3742)	-1.96 ± 0.10	-1.91 ± 0.08

3.4. Total Populations and Specific Frequencies

Next we estimate the total populations and specific frequencies of the GCSs. Here S_N is the number of clusters per unit galaxy luminosity (Harris & van den Bergh 1981; Harris

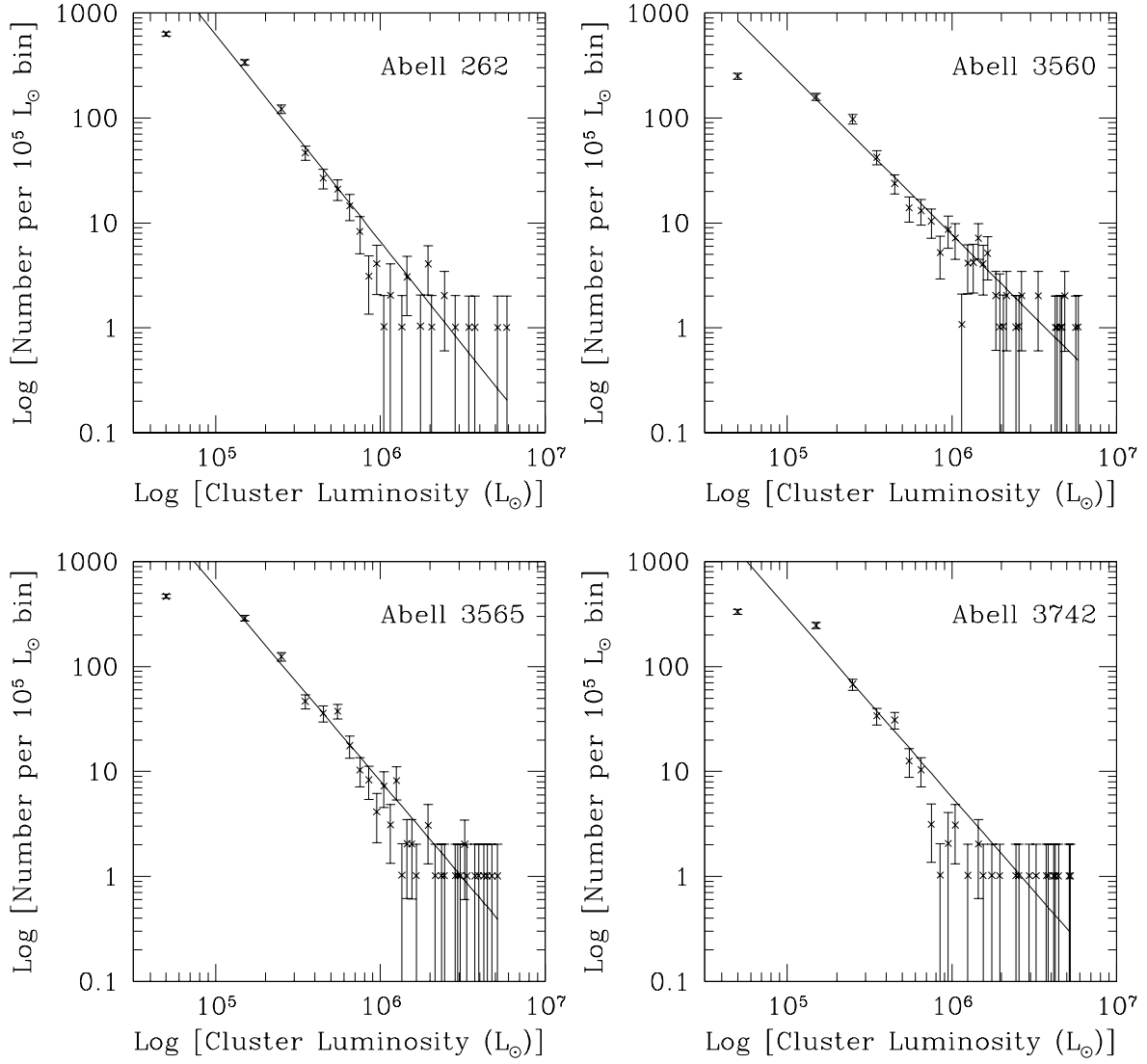


Fig. 5.— The data defining the luminosity distribution function (LDF). The solid lines are the least squares fits, with slopes given in Table 3. The lowest luminosity point has been excluded from the fit in all cases (see text).

et al. 1991):

$$S_N = N_{cl} \times 10^{0.4 (M_V^T + 15)}$$

where N_{cl} is the total number of clusters, and M_V^T is the integrated absolute magnitude of the host galaxy. S_N is found to differ among gE galaxies by more than an order of magnitude (Harris, Harris & McLaughlin 1998; Harris 2001). It is known that for cD-type and BCG galaxies the specific frequency increases systematically with the total galaxy luminosity, the size of the surrounding cluster of galaxies, and the X-ray halo gas mass (Blakeslee et al. 1997; Blakeslee 1999; Harris, Harris & McLaughlin 1998; McLaughlin 1999; Kavelaars 1999), albeit with a factor-of-two scatter that is not understood in detail.

We calculate the total number of clusters by integrating the radial profiles and scaling up the result by the fraction of the area under the bright half of the GCLFs (the completeness magnitude used for the radial profiles corresponds to 90% completeness, while for the GCLFs it is 50%). Following previously established convention (Harris 2001), the result is then doubled, which implicitly assumes that the GCLF is symmetric about the turnover magnitude. We can therefore think of specific frequency as equivalent to the number of *bright* clusters in a galaxy. Also, the value of S_N is fairly insensitive to the assumptions in the galaxy distance, because changes in distance will affect the calculated galaxy luminosity and total cluster population in the same sense (see Harris & van den Bergh (1981)).

The total populations along with the specific frequencies S_N are listed in Table 4. Figure 6 shows our results along with those from other gE galaxies previously published.

NGC 708 in A262 has the highest value for S_N , consistent with the fact that it is the only genuine cD-type galaxy of the four studied. The other three galaxies are central BCGs without the extended cD envelope, and have lower values for S_N . Somewhat of an outlier is IC 4296 in A3565, with a S_N value of 2.6, definitely on the low end for a such a high-luminosity elliptical. Its S_N is, however, similar to those of “field” ellipticals which are commonly thought to have formed by major mergers between relatively less cluster-rich disk galaxies. Even if the merging galaxies are quite gas-rich, a high- S_N elliptical would not necessarily result, since new field stars *and* star clusters both form during the merger, and the net ratio of clusters to field stars in the final merger product could either increase or decrease. The final S_N would be higher only if the efficiency of cluster formation was considerably enhanced over the cluster formation that took place in the original protogalactic epoch. In actually observed cases of recent disk/disk mergers, what appears to be emerging in every case is an elliptical with $S_N \sim 2$ (see Harris (2001) for more extensive discussion).

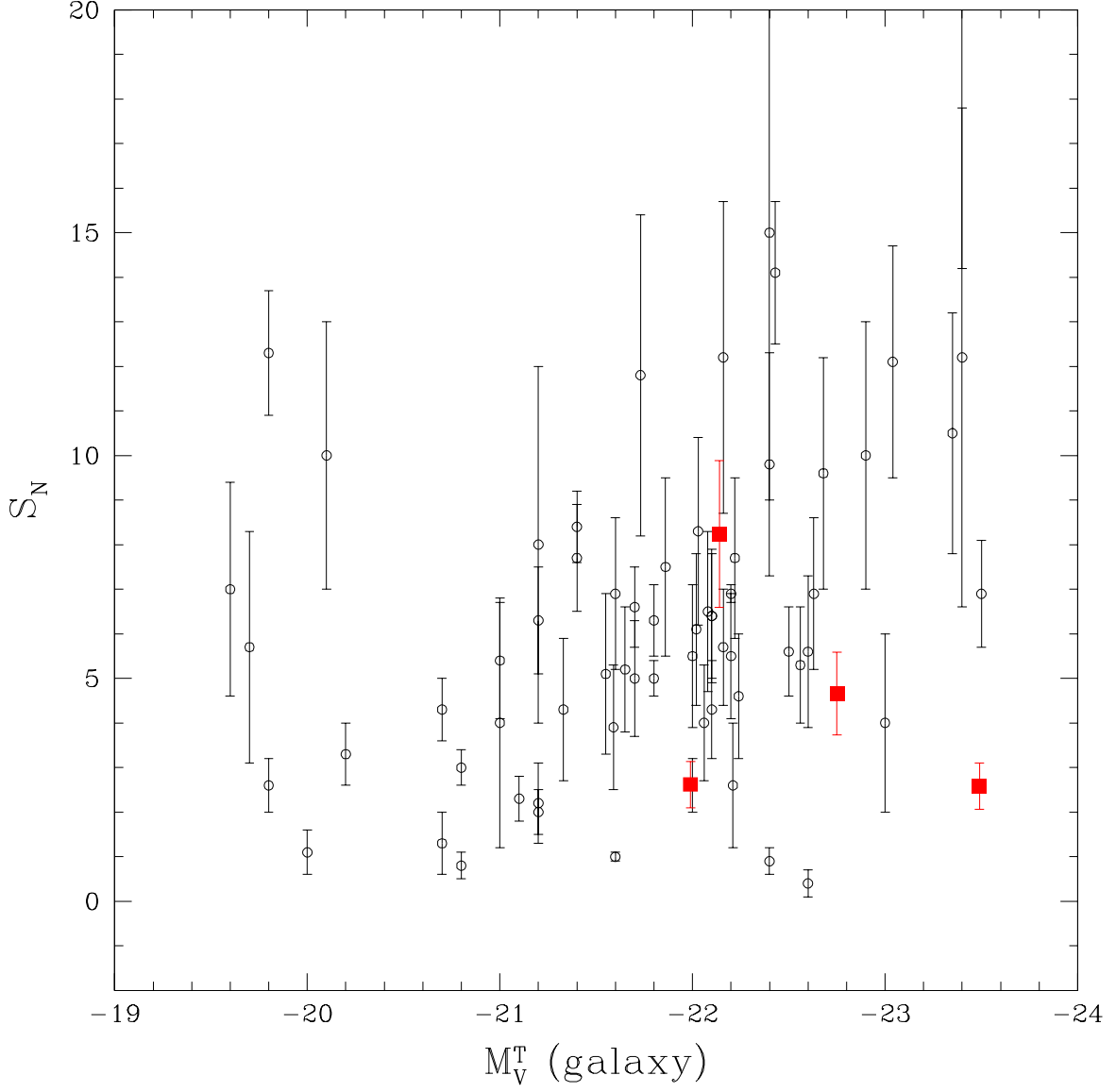


Fig. 6.— Specific Frequency S_N plotted against luminosity for elliptical galaxies. Squares represent our results for the BCGs, while open circles are results for other BCGs and gEs.

Table 4: Specific Frequency Data

Galaxy	M_V	N_d	S_n
N708 (A262)	-22.14	5924 ± 302	8.24 ± 1.65
N5193 (A3560)	-22.75	5878 ± 355	4.66 ± 0.93
I4296 (A3565)	-23.49	6400 ± 265	2.58 ± 0.52
N7014 (A3742)	-21.99	1634 ± 88	2.62 ± 0.52

3.5. The Hubble Diagram

By using our results for the GCLF turnover magnitudes, along with previous results for several other gE galaxies from the literature a classic “Hubble Diagram” of redshift cz against the apparent turnover magnitude V^0 of the GCLF can be constructed (see Harris (2001) and Kavelaars et al. (2000) for the first use of this diagram for GCLFs).

Hubble’s law states $cz = H_0 d$. This can be rewritten as:

$$\log(cz) = 0.2V^0 + \log H_0 - 0.2M_V^0 - 5$$

where M_V^0 is the GCLF turnover luminosity *for gE galaxies*, and H_0 is expressed in the usual units of $\text{km s}^{-1} \text{Mpc}^{-1}$. Plotting $\log(cz)$ against the apparent magnitude V^0 gives a straight line of slope 0.2, and a zeropoint which contains H_0 and M_V^0 .

The available data for a total of eleven BCG galaxies or groups are listed in Table 5 and plotted in Figure 7. The values for the Virgo and Fornax clusters are the weighted mean $\langle V^0 \rangle$ values of the individual galaxies (see Kavelaars et al. (2000)). The mean radial velocities of each galaxy or group are taken from Faber et al. (1989), Girardi et al. (1993), Huchra (1988), Binggeli, Popescu & Tammann (1993), Hamuy et al. (1996), Colless & Dunn (1996), and Lauer et al. (1998). Also, the recession velocities cz for the target galaxies assume a Local Group infall to Virgo of $250 \pm 100 \text{ km s}^{-1}$ (e.g., Ford et al. (1996); Hamuy et al. (1996); Jerjen & Tammann (1993), among many others).

The four galaxies we have investigated here fall well within the pattern established by the others (from Virgo at low redshift out to Coma at the highest redshift). A value of H_0 near $\simeq 70 \text{ km s}^{-1} \text{Mpc}^{-1}$, which represents a consensus of recent determinations (Freedman et al. 2001), along with $M_V^0 = -7.33$ (Kavelaars et al. 2000; Harris 2001), matches the total range of points within their measurement uncertainties.

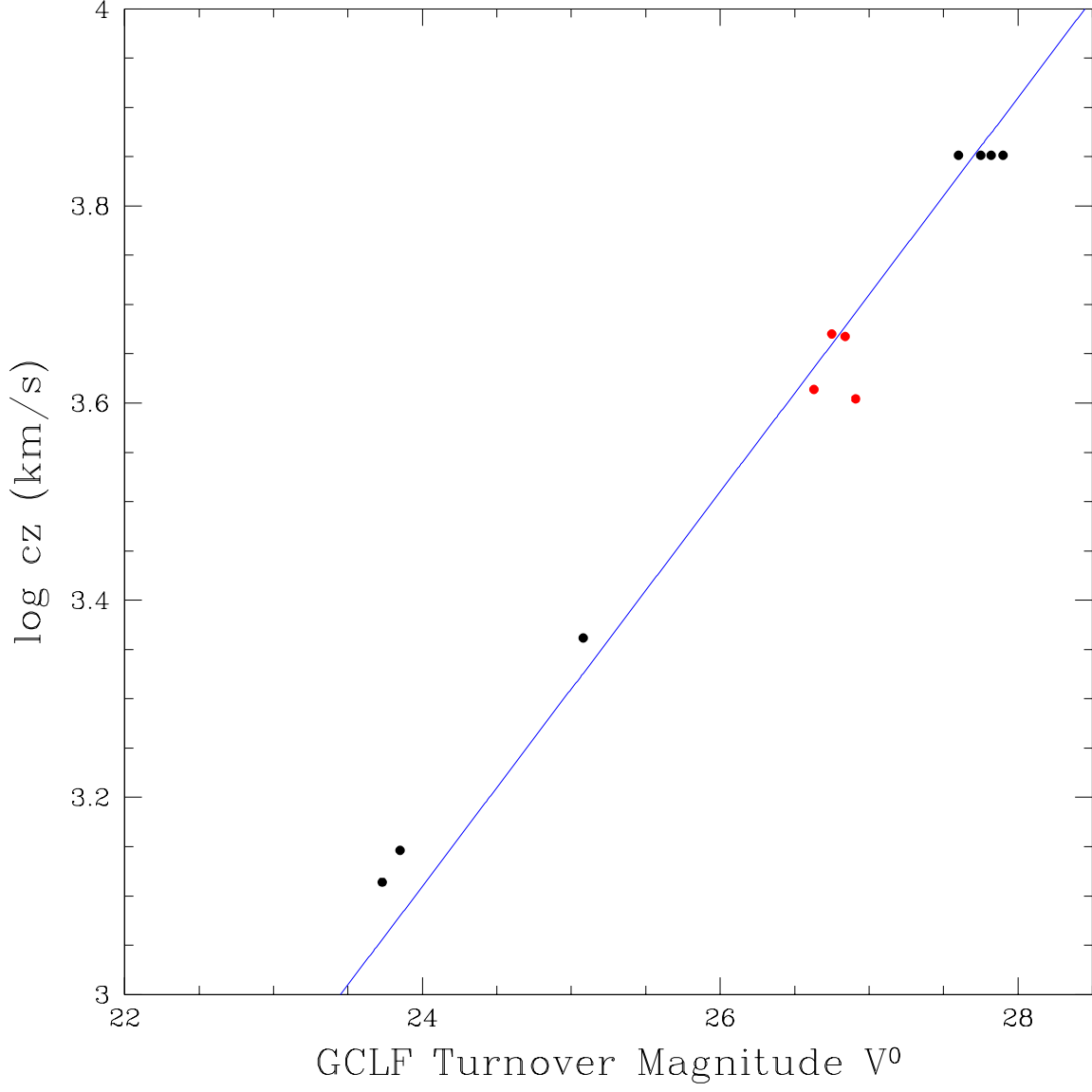


Fig. 7.— Hubble diagram for GCLF turnover magnitudes. The galaxy redshift cz is plotted against the apparent magnitude of the GCLF turnover, V^0 . The solid line is the expected relation for $H_0 = 70$ and an absolute turnover magnitude $M_V^0 = -7.33$ (see text).

Table 5: GCLF turnover magnitudes in distant ellipticals

Cluster	Galaxy	Redshift cz (km/s)	V^0 (GCLF)	Source
Virgo	6 gEs	1300	23.71 ± 0.03	1
Fornax	6 gEs	1400	23.85 ± 0.04	1
NGC 5846	NGC 5846	2300	25.08 ± 0.10	2
Coma	IC 4051	7100	27.75 ± 0.20	3
Coma	NGC 4874	7100	27.82 ± 0.12	1
Coma	NGC 4881	7100	> 27.6	4
Coma	NGC 4926	7100	27.90 ± 0.20	5
A 262	NGC 708	4650	26.84 ± 0.17	6
A 3560	NGC 5193	4020	26.91 ± 0.18	6
A 3565	IC 4296	4110	26.63 ± 0.16	6
A 3742	NGC 7014	4680	26.75 ± 0.19	6

Sources: (1) Kavelaars et al. (2000); (2) Forbes (1996); (3) Woodworth & Harris (2000); (4) Baum et al. (1995); (5) Kavelaars (2001); (6) this paper

4. Summary

Using deep I -band photometry from the *HST*/WFPC2 archive we have studied the globular cluster systems in NGC 708, NGC 5193, IC 4296 and NGC 7014, the BCGs in A262, A3560, A3565 and A3742. The photometry allowed us to construct the globular cluster luminosity functions for each of the above cluster systems, reaching to or just past the turnover point.

We have used a constrained χ^2 method to fit a Gaussian function to each of the four GCLFs, adopting a width $\sigma_V = 1.36$. The resulting background and extinction corrected V -band turnover magnitudes were found to be at $V^0 = 26.84 \pm 0.17$, 26.91 ± 0.18 , 26.63 ± 0.16 , 26.75 ± 0.19 respectively. These values improve on previous results of Lauer et al. (1998). The Hubble diagram generated from our GCLF turnover data combined with other material from the literature matches $H_0 \simeq 70 \text{ km s}^{-1} \text{ Mpc}^{-1}$.

We have obtained the luminosity and mass distribution functions for the GCSs. The slopes of the power law relations were found to be consistent with those for other giant elliptical galaxies, with the exception of NGC 5193 in A3560.

The total cluster populations N_{cl} and the specific frequencies S_N for each system were

calculated. The specific frequency of IC 4296 in A2565 is surprisingly low for its high luminosity, while the values for the other three galaxies fall within the established trend of specific frequency versus galaxy luminosity.

We would like to thank J.J.Kavalaars and Marcel VanDalfsen for useful comments and advice. This work was supported by the Natural Sciences and Engineering Research Council of Canada through a research grant to WEH.

REFERENCES

- Baum, W.A., et al. 1995, *AJ*, 110, 2537B
- Binggeli, B., Popescu, C.C., & Tammann, G.A. 1993, *A&AS*, 98, 275
- Blakeslee, J.P. 1999, *AJ*, 118, 1506
- Blakeslee, J.P., Tonry, J.L., & Metzger, M.R. 1997, *AJ*, 114, 482
- Colless, M., & Dunn, A.M. 1996, *ApJ*, 458, 435
- Elmegreen, B.G., & Efremov, Y.N. 1997, *ApJ*, 480, 235
- Faber, S.M., et al. 1989, *ApJS*, 69, 763F
- Forbes, D.A. 1996, *AJ*, 112, 954
- Ford, H.C., Hui, X., Ciardullo, R., Jacoby, G.H., & Freeman, K.C. 1996, *ApJ*, 458, 455
- Freedman, W.L., et al. 2001, *ApJ*, 553, 43
- Giovanelli, R., Haynes, M.P., & Chincarini, G.L. 1982, *ApJ*, 262, 442
- Girardi, M., Biviano, A., Giuricin, G., Mardirossian, F., & Mezzetti, M. 1993, *ApJ*, 404, 38
- Hamuy, M., Phillips, M.M., Suntzeff, N.B., Schommer, R.A., Maza, J., & Avil , R. 1996, *AJ*, 112, 2398
- Hanes, D.A., & Whittaker, D.G. 1987, *AJ*, 94, 906
- Harris, W.E. 1986, *AJ*, 91, 822
- Harris, W.E. 1990, *PASP*, 102, 966
- Harris, W.E. 2001, in *Star Clusters*, Saas-Fee Advanced School 28, ed. L Labhardt & B. Binggeli (Berlin: Springer), 223
- Harris W.E. 1991, *ARAA*, 29, 543
- Harris W.E., & van den Bergh, S. 1981, *AJ*, 86, 1627
- Harris W.E., Allwright, J.W.B., Pritchet, C.J., & van den Bergh, S. 1991, *ApJS*, 76, 115
- Harris, W.E., & Pudritz R.E. 1994, *ApJ*, 429, 177
- Harris, W.E., Harris, G.L.H., & McLaughlin, D.E. 1998, *AJ*, 115, 1801

- Harris W.E., Kavelaars, J.J., Hanes, D.A., Hesser, J.E., & Pritchett, C.J. 2000, *ApJ*, 533, 137
- Holtzman, J.A., et al. 1995, *PASP*, 107, 1065
- Huchra, J.P. 1988, in *ASP conf. Proc. 4, The Extragalactic Distance Scale*, ed. S. van den Bergh & C.J. Pritchett (San Francisco: ASP), 257
- Jerjen, H., & Tammann, G.A. 1993, *AAp*, 276, 1
- Kaisler, D., Harris, W.E., Crabtree, D.R., Richer, H.B. 1996, *AJ*, 111, 2224
- Kavelaars, J.J. 1999, *On the Relation Between Globular Cluster Specific Frequency and Galaxy Type, Galaxy Dynamics*, ASP Conference Series, ed. D.R. Merritt, M. Valluri, & J.A. Sellwood (San Francisco: ASP), vol. 182, 437
- Kavelaars, J.J., Harris, W.E., Hanes, D.A., Hesser, J.E., & Pritchett, C.J. 2000, *ApJ*, 533, 125
- Kavelaars, J.J. 2001, private communication
- Kron, R. 1980, *ApJS*, 43, 305
- Kundu, A., Whitmore, B.C., Sparks, W.B., Macchetto, F.D., Zepf, S.E., Ashman, K.M. 1999, *ApJ*, 513, 733
- Lauer, T.R., Tonry, J.L., Postman, M., Ajhar, E.A., & Holtzman, J.A. 1998, *ApJ*, 499, 577
- Lauer, T.R. 2001, private communication
- Mandushev, G., Spassova, N., & Staneva, A. 1991, *A&A*, 252, 94
- McLaughlin, D.E. 1994, *PASP*, 106, 47
- McLaughlin, D.E., & Pudritz, R.E. 1996, *ApJ*, 457, 578
- McLaughlin, D.E. 1999, *AJ*, 117, 2398
- McLaughlin, D.E. 2000, *ApJ*, 539, 618
- Mulchaey, J.S., Mushotzky, R.F., Burstein, D., Davis, D.S. 1996, *ApJ*, 456, 80
- Neill, D.J., Brodie, J.P., Craig, W.W., Hailey, C.J., Misch, A.A. 2001, *ApJ*, 548, 550
- Secker, J., & Harris, W.E. 1993, *AJ*, 105, 1358
- Stetson, P.B. 1994, *PASP*, 106, 250

- Whitmore, B.C., Sparks, W.B., Lucas, R.A., Macchetto, F.D., & Biretta, J.A. 1995, *ApJ*, 454, L73
- Whitmore, B.C. 1996, in *The Extragalactic Distance Scale*, ed. M. Livio, M. Donahue, & N. Panagia (Baltimore: STScI), 254
- Willmer C.N.A., et al. 1999, *AJ*, 118, 1131
- Woodworth, S., & Harris, W.E. 2000, *AJ*, 199, 2699